Available online at www.sciencedirect.com

ScienceDirect

Procedia Structural Integrity 2 (2016) 366–372

Structural Integrity Procedia

www.elsevier.com/locate/procedia

21st European Conference on Fracture, ECF21, 20-24 June 2016, Catania, Italy

Dynamic Fracture in Carbon-fibre Composites: Effect of Steel and Ice Projectiles

Laurence A. Coles[a], Anish Roy[a], Leonid Voronov[b], Sergey Semyonov[b], Mikhail Nikhamkin[b], Vadim V. Silberschmidt[a]

[a]*Wolfson School of Mechanical and Manufacturing Engineering, Loughborough University, Leicestershire, LE11 3TU, UK*
[b] *Aircraft Engines Department, Perm National Research Polytechnical University, Komsomolsky prosp., 29, 614000, Perm, Russian Federation*

Abstract

In this study the resultant ballistic dynamic response observed in a 2x2 twill weave T300 carbon fibre/epoxy composite flat-plate specimen is examined, using a combination of non-invasive analysis techniques. The study investigates deformation, damage and fracture following the impacts with both solid (steel) and fragmenting (ice) projectiles travelling with velocities of 70-90 m/s and 300-500 m/s, respectively. Digital image correlation was employed to obtain displacement data for the rear surfaces of the specimens in each experiment, and used to assess the effect of impact velocity and projectile material on the specimen's response. 3D X-ray computed tomography was used to image and visualize the resultant internal cloud of damage and fracture, initiated by dynamic loading in each specimen. It was shown that solid projectiles led to greater localized deformation and, in some cases, penetration, whereas fragmenting projectiles destroyed on impact resulted in more distributed loading leading to major front-surface damage depending on the depth on indentation before fragmentation.

Keywords: Ballistic Impact; CFRP; X-ray Tomography; Deformation; Damage

1. Introduction

The use of fibre-reinforced composites (FRCs) has increased considerably over the last few decades across many areas of application including automotive, aerospace, naval, defence, energy and sport. In many of these applications dynamic loading is a part of in-service conditions and can result in a wide range of damage. Some examples of dynamic loading may include low- and high-velocity impacts (in the range between 1 and 1000 m/s), ranging from flight at Mach 1-2 (300-600 m/s) of fighter jets or intercontinental ballistic missiles through clouds of debris or

10.1016/j.prostr.2016.06.047

hailstones, to lower-velocity impacts caused by debris on runways, railway lines, auto race tracks etc. As a result, developing a full understanding of these types of dynamic loading conditions and their effect on responses of FRCs is very important, in terms of both local and global distributions of deformation as well as initiation and evolution of the visible and hidden damage.

Over many years there have been a vast amount of research efforts towards characterising the response of FRCs under various dynamic loading conditions, but drawing comparisons between these studies is challenging – and often impossible – due to their major differences such as the type of specimens and, more importantly, employed experimental and analytical methodologies. In the past, some papers tried to surmise an overview of impact behavior such as the work conducted by Abrate (1991 & 1994), but analysis of considerable amounts of experimental data drew mostly qualitative conclusions on differences in methodology and used specimens together with broad statements on the effect of projectile mass and velocity on delamination behaviour.

In dynamic studies, it is important to understanding the type of loading conditions and character of temporal interaction with the specimen. For instance, a high volume of both experimental and numerical studies was focused on the resulting deformation, damage and fracture caused by solid projectiles (typically steel), but in recent years some efforts have been made towards understanding the impact process of ice projectiles (Pernas-Sánchez et al., 2015) and the effect on composite specimens of fragmentation on impact and resultant distribution of loading and dispersion of kinetic energy (Kim et al., 2003; Appleby-Thomas et al., 2011). But, typically, the analysis of the resultant damage is limited to a visual inspection of external surfaces, or a use of invasive techniques to study internal damage that could introduce additional damage complicating interpretation of results (Nunes et al., 2004; Sevkat, 2012; Shaktivesh et al., 2013; Yahaya et al., 2014). Some studies became investigating damage using X-ray tomography (Karthikeyan et al., 2013).

This paper presents the experimental case studies, in which carbon fibre/epoxy composite specimens were subjected to ballistic loading with steel and ice projectiles, in order to investigate and compare the resultant deformation, damage and fracture observed using digital image correlation and X-ray computed tomography (CT).

2. Experimental Setup

2.1. Materials and Specimens

The used in the test carbon-fibre-reinforced epoxy specimens, measuring approximately 195 mm x 195 mm with a thickness of 5.6 mm were fabricated from 10 plies of carbon-fibre fabric, pre-impregnated with a toughened epoxy matrix (IMP530R). The plies were formed to a laminate consisting of 2 surface plies (T300 3K) and 8 central bulking plies (T300 12K), with a 0/90° layup configuration. All specimens were manufactured using the autoclave process, cured at 120°C with a ramp rate of 1.5°C/min and a soak time of 160 minutes at a pressure of 90 Psi under full vacuum. A theoretical density of the produced specimens was 1600 kg/m^3.

2.2. Pneumatic Gun and Specimen Setup

The investigation was performed on specially developed ballistic experimental apparatus utilising a pneumatic gun. The CFRP specimens were installed into a 4-axis positioning system, and aligned with the barrel resulting in a cantilever clamping regime with all specimens being subjected to a perpendicular impact (as shown in Figure 1). The projectile was accelerated to the required speed in the barrel using compressed air, and muzzle velocity measurements were collected using a light gate device installed between the specimen and the end of barrel. Projectile velocities were then determined based on the time difference between the signal peaks from the light gates; the experiment was controlled by a PC via a PXI system (National Instruments). The impact process was captured using two high-speed cameras (Photron Fastcam SA5) configured in two arrangements, the first to capture the front and top views at 25,000 - 50,000 frames per second while the second captured the rear surface for digital image correlation (DIC) using the VIC-3D (Correlated Solutions) system at 60,000 frames per second.

2.3. Projectile and Experiment Parameters

All the solid (steel) projectiles were measured to be 23.8 mm diameter with a weight of 54.7 g, and the fragmenting ice (hailstone imitation) projectiles had a diameter 25 mm with a weight of 7.5 g at a temperature of -20°C. The impact velocities were chosen to produce three levels of damage within the specimens – minor, medium and major with penetration, and were determined in preliminary calibration experiments to be approximately 60, 75 and 90 m/s for the steel projectiles and 300, 400 and 500m/s for the ice ones.

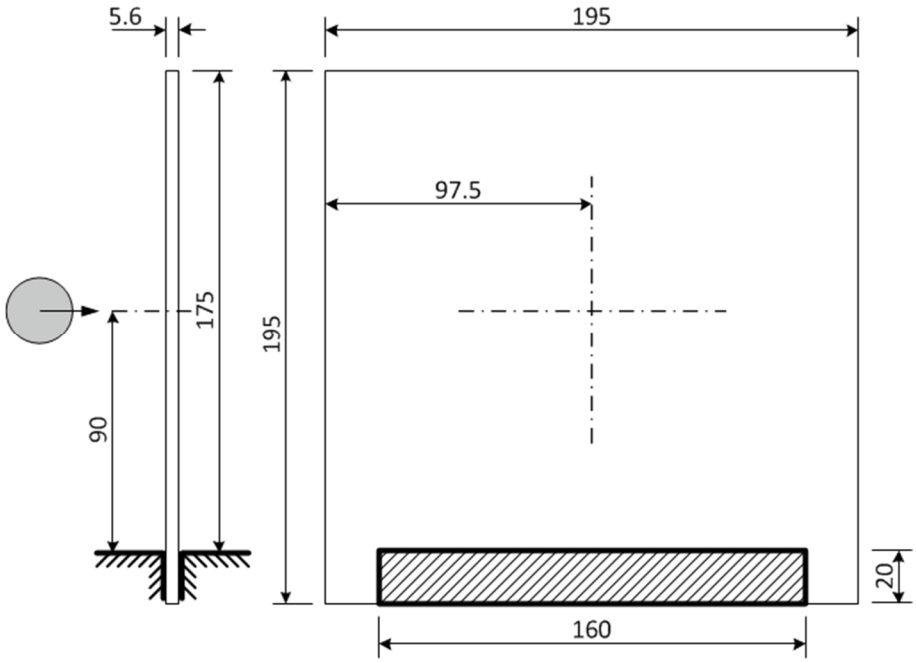

Fig. 1. Ballistic impact regime and cantilever clamping fixture

2.4. Configuration of X-ray Tomography Scans

All the specimens were inspected using a Metris 160 H-XT XCT system to investigate the extent of the internal damage and its spatial distribution. Each scan was conducted at 140 kV and 130 µA using a tungsten target, with 2650 radiography projections taken over the 360° rotation for each specimen at an exposure of 500 ms. In order to reduce granular noise, 8 images where taken and averaged per projection. The total volume scanned for each specimen was 180 mm x 140 mm x 20 mm at a resolution of 97 µm.

3. Experimental results and discussion

Following the experiment case studies, typical impacts for both the steel and ice projectiles can be seen in Figure 2, where the ice projectile initially indented the specimen before fragmenting within it causing major widespread fracture and delamination of the first few plies. The steel projectile resulted in major indentation before full penetration, as expected, leaving more localised damage and fracture when compared to those of the ice projectiles.

3.1. Deformation Analysis

It is clear from analysing global displacement in the steel (solid) projectile impacts, that the rigid nature of the projectile material caused more defined indentation in the specimen before the transition into global flexural bending. This initial indentation was still present in the case of the ice projectiles, but it is clear that the local indentation was more gradually transitioned to the distributed loading upon fracture and fragmentation of ice leading to global flexural bending. This difference resulted in varying curvature of the specimens at different stages of loading with teo types of projectiles: for the steel ones the specimen's curvature was more subtle, with gradual transitions between concave and convex forms, whereas for the ice projectile the transition in curvature were more noticeable. As a result of the ice projectile fragmenting on impact, the transition to distributed loading caused a reduction in the out-of-plane displacement and resulted in minor damage and fracture observed at the rear surface. In impacts with the steel projectile at lower energies, the out-of-plane displacement was found to be greater leading to more significant damage at the rear surface of the specimens.

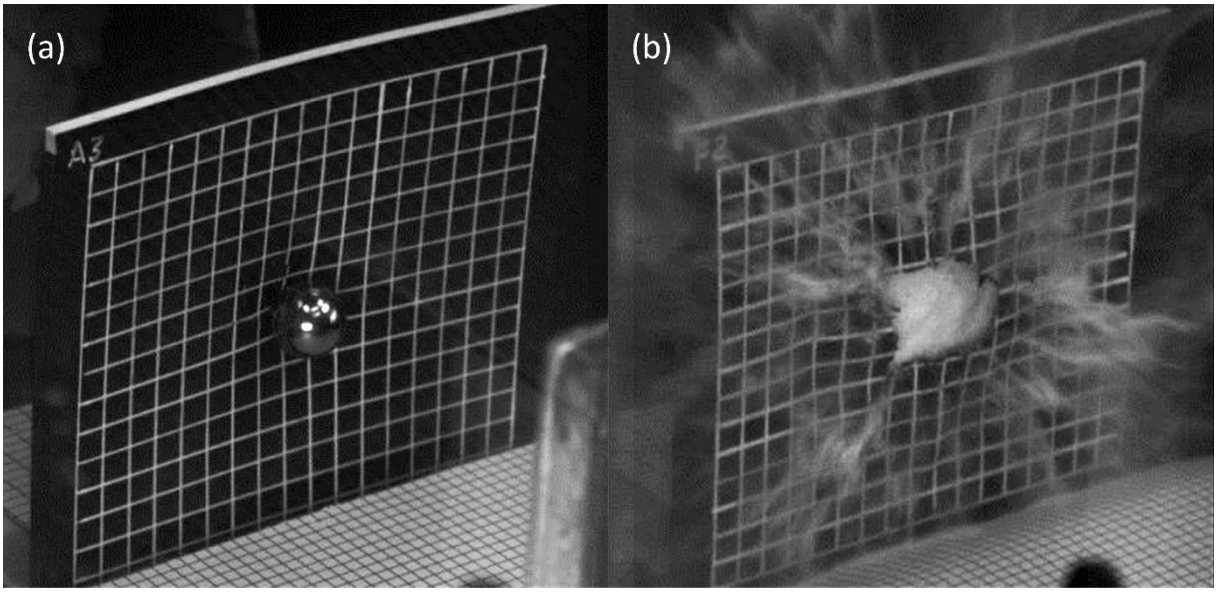

Fig. 2. Typical impact behavior of solid steel projectile at 0.40 ms (a) and fragmenting ice projectile at 0.19 ms (b)

When considering the localised deformation behaviour and the normalised response of each specimen, these differences in dynamic response and specimen curvature in the process of loading became apparent. This demonstrates that both projectiles can result in considerable damage and fracture of the CFRP specimens, and highlights the requirements for detailed analysis of this damage for specific impact interactions. Additionally, it is clear that the maximum out-of-plane displacement increased with the growth of projectile velocity (energy), as expected. The same can be said about the time to the maximum displacement (although the trend could not be identified as clearly due to the limitations related to time resolution, directly linked to the camera's frame rate), with the increased velocities (energies) resulting in a reduced magnitudes of this time.

3.2. Damage Analysis

Following ballistic impact tests with the solid and fragmenting projectiles, each specimen was inspected and as a result showed two very distinct types of visual damage. For the steel projectiles, a highly localised and, therefore, more penetrating damage interaction was observed, while for the fragmenting projectiles a more widespread damage interaction with the front surface of the specimen with some signs of the early stages of penetration. An example of the damage clouds observed in X-ray CT scans of two major damage loading cases can be seen in Figure 3, both for

the solid (Fig. 3a) and fragmenting (Fig. 3b) projectiles. The transparent 3D rendered tomograms allow the damage clouds to be assessed in terms of increasing cloud area and greyscale intensity; the greater the intensity of the grey-scale value, the higher the accumulation of damage through the thickness of the specimen. For instance, the specimen impacted with the solid projectile shows a dark-grey zone toward the centre indicating greater penetration-induced damage, whereas the fragmenting (ice) projectiles generated catastrophic damage across the whole front surface and first few plies causing a more distributed intensity gradient. From the analysis of the scans and employing additional 2D cross sections and 3D images it became clear that the main damage modes observed were either delamination or damage and fracture in tensile plies and fibre, but at the resolution employed it was not possible to accurately determine any other damage mechanisms. These scans also confirmed the localized indentation and damages for the steel projectiles, and clearly showed the widespread damage covering most of the specimen in the impact with the fragmenting projectiles.

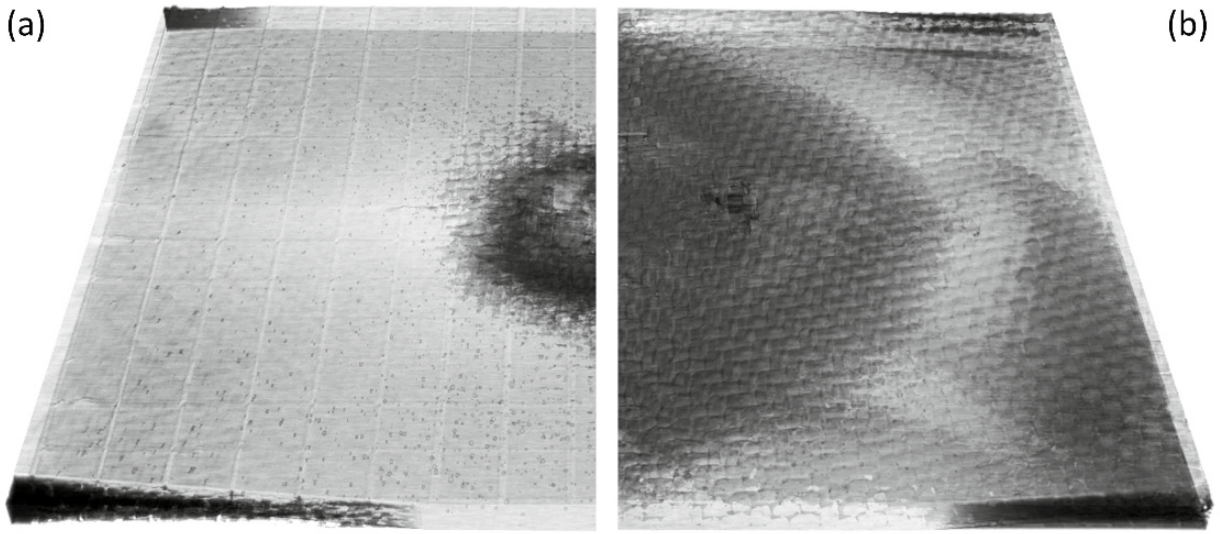

Fig. 3. Typical examples of internal damage cloud in specimens after impacts with solid (steel) projectile (a) and fragmenting (ice) projectile (b)

This damage patterns and its observations confirmed previous conclusions regarding the effect of impact energy (velocity) in impacts with two different types of projectiles: in the case of steel projectiles, the damage cloud remained highly localised even with increasing impact energy, whereas for the ice projectile the damage cloud increased more clearly in this process due to the higher level of initial indentation. This demonstrates that the energy of fragmenting projectiles has a stronger effect on the induced damage, affecting the damage propagation throughout the specimen in the impact event.

Analysis of the virtual 2D horizontal and vertical cross sections of each specimen allowed approximate measurements of damage zones down to the features observable at 97 μm. Figure 4 shows the final averaged distribution of damage against the averaged maximum out-of-plane displacement for various impact velocities. Although these displacements were not available for the major damage case, an increasing trend in this maximum displacement can clearly be seen, as expected. Also, as mentioned previously, when observing the damage clouds caused by the solid projectiles, the average area increased but the damage zone remained highly localised. In contrast, for the fragmenting projectiles, the impact energy clearly resulted in a substantial increase in the damage cloud area in the tested composite panels.

4. Conclusions

For projectiles of the same size, an impact with a solid (steel) one demonstrated more defined indentation of the composite plates before their transition into global flexural bending, whereas fragmenting (ice) projectiles produced

initial indentation but, upon fragmentation, any local indentation was more gradually transitioned to distributed loading leading to global flexural bending. Comparing each of the loading conditions showed that projectiles of the same material will produce similar responses of the impacted specimen, even at different energy levels (within the studied range). Oppositely, two projectiles of different materials and, importantly, a character of interaction, showed differing levels of indentation of the specimens, even at lower energy levels. The transition from indentation to global flexural bending also changes with projectile material, affecting the curvature of the specimen throughout its deformation.

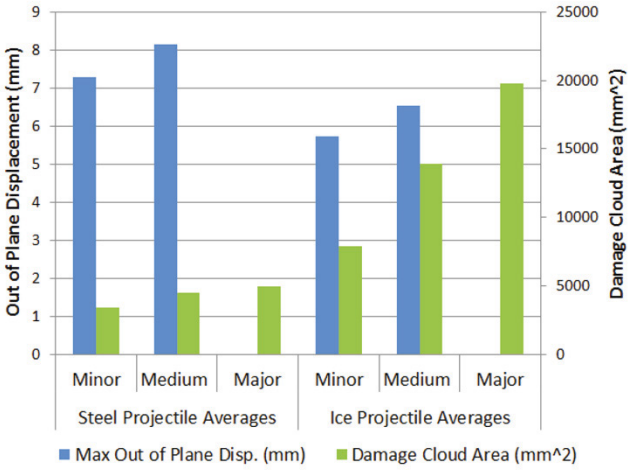

Figure 4. Maximum out of plane displacement for both the solid steel and fragmenting ice projectiles

Damage at the rear surface of the specimens occurs much sooner when the projectile is formed of solid (steel) rather than that of the fragmenting (ice) projectile, this is likely due to the almost instantaneous fragmentation of the ice projectile on impact causing more widely distributed loading and therefore a longer impact duration even at the clearly higher impact energies. Although the fragmenting (ice) projectile does mitigate the penetration of the specimen, the partial indentation shortly followed by the destruction of the projectile cause the delamination and removal of the first 2-3 plies from the front surface for the major damage case which is still regarded as major damage to the specimen. Finally the impact energy to shown to have little effect on the damage cloud for solid (steel) projectiles, while for the fragmenting (ice) projectiles the increasing impact energy demonstrates substantial increases in the damage clouds seen.

5. References

Abrate, S., 1991. Impact on Laminated Composites. ASME: Applied Mechanics Reviews 44, 155-190.

Abrate, S., 1994. Impact on Laminated Composites: Recent Advances. ASME: Applied Mechanics Reviews 47, 517-544.

Appleby-Thomas, G. J., Hazell, P. J., Dahini, G., 2011. On the response of two commercially-important CFRP structures to multiple ice impacts. Composite Structures 93, 2619-2627.

Karthikeyan, K. et al., 2013. The effect of shear strength on the ballistic response of laminated composite plates. European Journal of Mechanics - A/Solids 42, 35-53.

Kim, H., Welch, D. A. & Kedward, K. T., 2003. Experimental investigation of high velocity ice impacts on woven carbon/epoxy composite panels. Composites Part A: Applied Science and Manufacturing 34, 25-41.

Nunes, L. M., Paciornik, S. & d'Almeida, J. R. M., 2004. Evaluation of the damaged area of glass-fiber-reinforced epoxy-matrix composite materials submitted to ballistic impacts. Composites Science and Technology 64, 945-954.

Pandya, K. S., Pothnis, J. R., Ravikumar, G. & Naik, N. K., 2013. Ballistic impact behavior of hybrid composites. Materials & Design 44, 128-135.

Pernas-Sánchez, J., Artero-Guerrero, J. A., Varas, D. & López-Puente, J., 2015. Analysis of Ice Impact Process at High Velocity. Experimental Mechanics 55, 1669-1679.

Sevkat, E., 2012. Experimental and numerical approaches for estimating ballistic limit velocities of woven composite beams. International Journal of Impact Engineering 45, 16-27.

Shaktivesh, Nair, N. S., Sesha Kumar, C. V. & Naik, N. K., 2013. Ballistic impact performance of composite targets. Materials & Design 51, 833-846.

Yahaya, R. et al., 2014. Quasi-static penetration and ballistic properties of kenaf–aramid hybrid composites. Materials & Design 63, 775-782.